Theory of the Lorentz force flowmeter

View the article online for updates and enhancements.

You may also like

Theory of the Lorentz force flowmeter

André Thess[1], Evgeny Votyakov[1], Bernard Knaepen[2] and Oleg Zikanov[3]

[1] Fakultät für Maschinenbau, Technische Universität Ilmenau, Postfach 100565, 98684 Ilmenau, Germany
[2] Université Libre de Bruxelles, Service de Physique Théorique et Mathématique, Campus Plaine—CP231 Boulevard du Triomphe, 1050 Brussels, Belgium
[3] Department of Mechanical Engineering, University of Michigan—Dearborn, 4901 Evergreen Road, Dearborn, MI 48128-1491, USA
E-mail: thess@tu-ilmenau.de

Abstract. A Lorentz force flowmeter is a device for the contactless measurement of flow rates in electrically conducting fluids. It is based on the measurement of a force on a magnet system that acts upon the flow. We formulate the theory of the Lorentz force flowmeter which connects the measured force to the unknown flow rate. We first apply the theory to three specific cases, namely (i) pipe flow exposed to a longitudinal magnetic field, (ii) pipe flow under the influence of a transverse magnetic field and (iii) interaction of a localized distribution of magnetic material with a uniformly moving sheet of metal. These examples provide the key scaling laws of the method and illustrate how the force depends on the shape of the velocity profile and the presence of turbulent fluctuations in the flow. Moreover, we formulate the general kinematic theory which holds for arbitrary distributions of magnetic material or electric currents and for any velocity distribution and which provides a rational framework for the prediction of the sensitivity of Lorentz force flowmeters in laboratory experiments and in industrial practice.

Contents

1. Introduction

The measurement of velocity in liquid metals is a notoriously difficult problem because these materials are opaque and often hot and aggressive. Especially in situations where the liquid metals are at high temperature, as in metallurgy, the development of reliable contactless velocity measurement methods has far reaching consequences. The goal of the present work is to establish the theoretical foundations of Lorentz force velocimetry—an electromagnetic flow measurement method that is based on exposing a flow to a magnetic field and measuring the force acting on the magnetic field generating system (cf [1] and references therein).

Flow measurement using magnetic fields has a long history. It started in 1832 when Michael Faraday attempted to determine the velocity of the Thames river [2]. Faraday's method which consists of exposing a flow to a magnetic field and measuring the induced voltage using two electrodes has evolved into a successful commercial application known as the inductive flowmeter. The theory of such devices has been developed and comprehensively summarized by [3]. While inductive flowmeters are widely used for flow measurement in fluids at low temperatures such as beverages, chemicals and wastewater, they are not suited for flow measurement in metallurgy. Since they require electrodes to be inserted into the fluid, their use is limited to applications at temperatures far below the melting points of practically relevant metals. Consequently there have been several attempts to develop flow measurement methods which do not require any mechanical contact with the fluid. Among them is the eddy current flowmeter [4] which measures flow-induced changes in the electric impedance of coils interacting with the
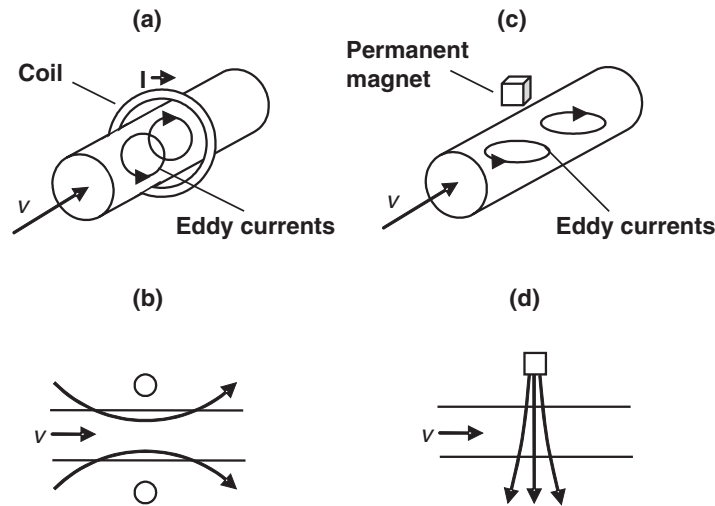
Figure 1. Principle sketch of Lorentz force velocimetry: arrangement of the coil (a) and structure of the primary magnetic field (b) for a longitudinal flux flowmeter. (c, d) Same for a transverse flux flowmeter. The magnetic-field-generating system will also be called the *magnet system* for brevity.

flow. More recently, a noncontact method was proposed [5, 6] in which a magnetic field is applied to the flow and the velocity is determined from measurements of flow-induced deformations of the applied field.

The present paper is devoted to a method whose origin goes back to [3] (chapter 4.2 and references therein, see also [7]), which has been further developed by [8]–[13] and for which the term Lorentz force velocimetry has been proposed by [1]. The goal of the present work is to explain the principles of this method using several simple models and to formulate the theory which is necessary to perform sensitivity analyses and optimizations for practical applications. The method is examined and analysed here using the example of flux measurements in a flow of an incompressible fluid in a circular pipe at low magnetic Reynolds number. However, the theory can be readily generalized to channels with arbitrary cross-sections and flows with finite magnetic Reynolds number. The specific examples to be discussed in sections 3 and 4 will focus on measurements of a global quantity, namely the volume flux. Devices which perform this task will be referred to as Lorentz force flowmeters. The example treated in section 5 as well as the general theory presented in section 6 apply to both volume flux measurements and local velocity measurements. This general method is referred to as Lorentz force velocimetry.

2. Basic principles

When an electrically conducting fluid moves across magnetic field lines, which are either produced by a current-carrying coil (as in figure 1(a)) or by a permanent magnet (as in figure 1(c)), the induced eddy currents lead to a Lorentz force which brakes the flow. The Lorentz force density is roughly

$$f \sim \sigma v B^2 \qquad (1)$$

where σ is the electrical conductivity of the fluid, v is its velocity and B is the magnitude of the magnetic field. This phenomenon is well known [14]–[16] and has found a variety of applications for flow control in metallurgy and crystal growth [17]. Equally obvious but less widely appreciated is the fact that by virtue of Newton's law, an opposite force acts upon the magnetic-field-generating system and drags it along the flow direction as if the magnetic field lines were invisible obstacles. A Lorentz force flowmeter is a device which determines the flow rate from a measurement of this force.

Lorentz force flowmeters can be constructed in two different ways. They can be designed as static flowmeters where the magnet system is at rest and one measures the force acting on it. Alternatively, they can be designed as rotary flowmeters where the magnets are arranged on a rotating wheel and the spinning velocity is a measure of the flow velocity.

Obviously, the force acting on a Lorentz force flowmeter depends both on the velocity distribution and on the shape of the magnet system. For both static and rotary flowmeters it is therefore equally important to answer the following two questions: (i) What is the force on the magnet system for a given velocity distribution? (ii) How does the presence of the magnetic field affect the flow? The focus of the present work will be on the first question which will be termed the *kinematic problem* (as opposed to the *dynamic* problem that takes into account the back-reaction of the Lorentz force on the flow). The second question will be briefly addressed in section 3.2 where we compare the results of kinematic and dynamic numerical simulations. Before engaging in a systematic analysis of Lorentz force flowmeters it is important to gain a qualitative understanding of the basic phenomena.

We denote the electric current in the coil of figure 1(a) by $\mathbf{J}(\mathbf{r})$ and call it the *primary current*. The magnetic field $\mathbf{B}(\mathbf{r})$ due to primary current will be referred to as the *primary magnetic field*. In figure 1(c) the primary field is produced by a permanent magnet characterized by the spatial distribution $\mathbf{M}(\mathbf{r})$ of magnetization density. This quantity can be described by a fictituous distribution of primary currents $\mathbf{J}(\mathbf{r})$ as will be detailed in section 6, so both electromagnets and permanent magnets can be treated within the same mathematical framework. The motion of the fluid under the action of the primary field induces eddy currents which are sketched in figures 1(a) and (c). They will be denoted by $\mathbf{j}(\mathbf{r})$ and are called *secondary currents*. The interaction of the secondary current with the primary magnetic field is responsible for the Lorentz force

$$\mathbf{F}_f = \int_f \mathbf{j} \times \mathbf{B} \mathrm{d}^3\mathbf{r} \tag{2}$$

which brakes the flow.

The secondary currents create a magnetic field $\mathbf{b}(\mathbf{r})$, the *secondary magnetic field*. The interaction of the primary electric current with the secondary magnetic field gives rise to the Lorentz force

$$\mathbf{F}_m = \int_m \mathbf{J} \times \mathbf{b} \, \mathrm{d}^3\mathbf{r} \tag{3}$$

which acts upon the magnet system. We would like to repeat that this formula also holds for a permanent magnet because its magnetic field can be represented by fictitious electric currents. In (2) the integration extends over the domain of the fluid, whereas in (3) the integration is over the volume of the coil or of the permanent magnet. Strictly speaking, the force on a permanent magnet is the Kelvin force but we will use the term Lorentz force throughout.

A key element of Lorentz force velocimetry is the relation

$$\mathbf{F}_m = -\mathbf{F}_f \tag{4}$$

called *reciprocity principle* which states that the electromagnetic forces on the fluid and on the magnet system have the same magnitude and act in opposite direction. To verify this relation we start from the observation that the total Lorentz force due to the interaction of a localized distribution of electric currents with its own magnetic field is zero. This relation holds independently for the primary fields, the secondary fields and the total fields and has the form

$$\int \mathbf{J} \times \mathbf{B} \, d^3\mathbf{r} = \int \mathbf{j} \times \mathbf{b} \, d^3\mathbf{r} = \int (\mathbf{J} + \mathbf{j}) \times (\mathbf{B} + \mathbf{b}) \, d^3\mathbf{r} = \mathbf{0}. \tag{5}$$

Expansion of the third integral and the use of the first two integrals immediately lead to the relation (4). A consequence of the reciprocity principle is that one can choose among two alternatives for the computation of the Lorentz force and select the one which is more convenient for the probem at hand. We will illustrate this issue in the next sections.

Before turning to the analysis of specific cases we wish to emphasize that the Lorentz force (1) is proportional to the square of the magnetic field. This is a consequence of the fact that the magnet system simultaneously acts as a source of the primary and a sensor of the secondary field. Hence the sensitivity of a Lorentz force flowmeter increases more quickly with increasing magnetic field than in methods based on the measurement of magnetic field perturbations (see e.g. [5]). In the latter case the sensitivity increases only linearly with the magnetic field.

3. Longitudinal flux flowmeter

3.1. Analytical theory for laminar flows

We start our analysis with the case of a unidirectional flow of a fluid with electrical conductivity σ in a circular pipe with radius R which is subjected to an axisymmetric magnetic field given by

$$\mathbf{B} = B_r(r, z)\mathbf{e}_r + B_z(r, z)\mathbf{e}_z, \tag{6}$$

see figure 1. We use cylindrical coordinates (r, φ, z) with the unit vectors $\mathbf{e}_r$, $\mathbf{e}_\varphi$ and $\mathbf{e}_z$ where the coordinate z points in the streamwise direction. The magnetic field (6) has to satisfy the condition $\nabla \cdot \mathbf{B} = 0$ but can otherwise be arbitrary. Flowmeters whose magnetic field is axisymmetric and whose symmetry axis coincides with that of the pipe will be called longitudinal flux flowmeters. We consider steady flows of the form

$$\mathbf{v} = v(r)\mathbf{e}_z. \tag{7}$$

To compute the Lorentz force in the framework of the kinematic theory we start with Ohm's law

$$\mathbf{j} = \sigma(\mathbf{E} + \mathbf{v} \times \mathbf{B}). \tag{8}$$

In the case of low magnetic Reynolds numbers we can use the primary field given by equation (6) instead of the full magnetic field and represent the electric field using an electric potential

$\mathbf{E} = -\nabla\Phi$. Taking the divergence of Ohm's law we obtain

$$\nabla^2 \Phi = \mathbf{B} \cdot \omega \tag{9}$$

where $\omega = \nabla \times \mathbf{v}$ is the vorticity. For flows of the form (7) the vorticity is parallel to $\mathbf{e}_\varphi$ so the right-hand side of (9) vanishes. Since the electric potential has to satisfy the homogeneous boundary conditions $\Phi = 0$ at $r = 0$ and $\partial\Phi/\partial r = 0$ at $r = R$ we have $\Phi = 0$, i.e. the potential vanishes. We can therefore immediately obtain the eddy currents

$$\mathbf{j} = \sigma v(r) B_r(r, z) \mathbf{e}_\varphi \tag{10}$$

which are purely azimuthal and parallel to the wall of the pipe. The Lorentz force density acting on the fluid is given by

$$\mathbf{f} = \mathbf{j} \times \mathbf{B}. \tag{11}$$

We are only interested in the z-component of the total Lorentz force whose value will be denoted by F and is obtained by integrating the z-component of $\mathbf{f}$ over the volume of the pipe. The integral of the other components of the Lorentz force vanishes by symmetry. The resulting expression for F reads

$$F = -2\pi\sigma \int_{-\infty}^{+\infty} \int_0^R v(r) B_r^2(r, z) r \, \mathrm{d}r \, \mathrm{d}z. \tag{12}$$

Since B_r^2 is positive, the force is always directed opposite to the flow provided that $v(r) \geqslant 0$ everywhere (i.e. F and the volume flux $\int vr \, \mathrm{d}r$ have opposite signs).

    The force can be evaluated explicitly if the magnetic field has the form

$$B_r = \frac{3B_0}{2L^2} \frac{rz}{(1 + z^2/L^2)^{5/2}}, \qquad B_z = B_0 \frac{1}{(1 + z^2/L^2)^{3/2}}. \tag{13}$$

This expression describes the magnetic field produced by a single coil with radius L wrapped around the pipe for the special case $R \ll L$ (see e.g. [18]). The field has its maximum B_0 on the axis of the cylinder at $z = 0$. The integration over the magnetic field can be performed analytically and the total Lorentz force becomes

$$F = -\frac{45\pi^2}{256} \frac{\sigma B_0^2}{L} \int_0^R v(r) r^3 \, \mathrm{d}r. \tag{14}$$

This equation shows that the force on the longitudinal flux flowmeter depends on the shape of the velocity profile and the flowmeter samples the velocity close to the wall. In order to analyse how strongly the force depends on the shape of the velocity profile let us analyse this expression for some particular cases. It is convenient to express the velocity profile as $v(r) = v_0 g(r/R)$ with a nondimensional shape function $g(\xi)$ whose normalization $\int g(\xi)\xi \, \mathrm{d}\xi = 1/2$ is such that the volume flux through the pipe equals $\pi R^2 v_0$, thus giving the velocity scale v_0 the meaning of the average velocity. With this step done, the force can be expressed as

$$F = -\frac{45\pi^2}{256} \frac{\sigma v_0 B_0^2 R^4}{L} S \tag{15}$$

where the quantity

$$S = \int_0^1 g(\xi)\xi^3 \, \mathrm{d}\xi \tag{16}$$

can be interpreted as the sensitivity of the flowmeter.

The simplest case pertains to solid-body translation for which $v(r) = v_0$ and thus $g(\xi) = 1$ which gives

$$S = \tfrac{1}{4}. \tag{17}$$

Next we consider the Poiseuille flow which is described by $g(\xi) = 2(1 - \xi^2)$. After a straightforward integration we obtain

$$S = \tfrac{1}{6} \tag{18}$$

which shows that the force from a Poiseuille flow is by a factor 2/3 smaller than for a moving solid body.

Let us now analyse the more general one-parameter family of profiles

$$g(\xi) = \beta(\alpha) \ln\left[1 + \alpha(1 - \xi^2)\right], \tag{19}$$

with $\beta(\alpha) = \alpha/[(1 + \alpha)\ln(1 + \alpha) - \alpha]$ to ensure the normalization $\int g(\xi)\xi \, \mathrm{d}\xi = 1/2$. For $\alpha \to 0$ this profile obeys $g(\xi) \to 2(1 - \xi^2)$, i.e. it is Poiseuille-shaped, whereas for $\alpha \to \infty$ we have $g(\xi) \to 1$ as for solid-body translation except for $\xi = 1$ where $g = 0$. Moreover, for $\alpha \gg 1$ this profile has the virtue of approximating the velocity distribution of turbulent pipe flow where α is proportional to the Reynolds number as will be detailed below. Using symbolic integration it is straightforward to work out the expression

$$S(\alpha) = \frac{2(1 + \alpha)^2 \ln(1 + \alpha) - \alpha(2 + 3\alpha)}{8\alpha[(1 + \alpha)\ln(1 + \alpha) - \alpha]}, \tag{20}$$

for the sensitivity. It is reassuring to verify that $S \to 1/6$ for $\alpha \to 0$ and $S \to 1/4$ for $\alpha \to \infty$, as obtained previously. Figure 2 shows that $S(\alpha)$ smoothly connects the limiting cases of Poiseuille flow and solid-body translation.

Although the force on the Lorentz force flowmeter depends on the shape of the profile, the following numerical example shows that this dependence is weak. For turbulent flows the parameter appearing in the model profile (19) can be approximately identified with the Reynolds number $Re = 2Rv_0/\nu$ via $\alpha = \kappa(\lambda/2)^{1/2} Re$ where $\kappa = 0.41$ is the von-Karman constant and the friction factor λ is a solution of Prandtl's universal equation $\lambda^{-1/2} = 2.0 \log[Re\,\lambda^{1/2}] - 0.8$ (for a discussion of the coefficients in the light of recent experiments see [19]). Let us compare the sensitivities for $Re = 10^5$ and $Re = 10^6$ which represent typical values in metallurgy. For $Re = 10^5$ we have $\lambda = 0.01799$, $\alpha = 3889$ and $S = 0.2329$, whereas for $Re = 10^6$ we obtain $\lambda = 0.01165$, $\alpha = 31290$ and $S = 0.2366$. Thus the sensitivities differ by only 2% when the Reynolds number changes by one order of magnitude.
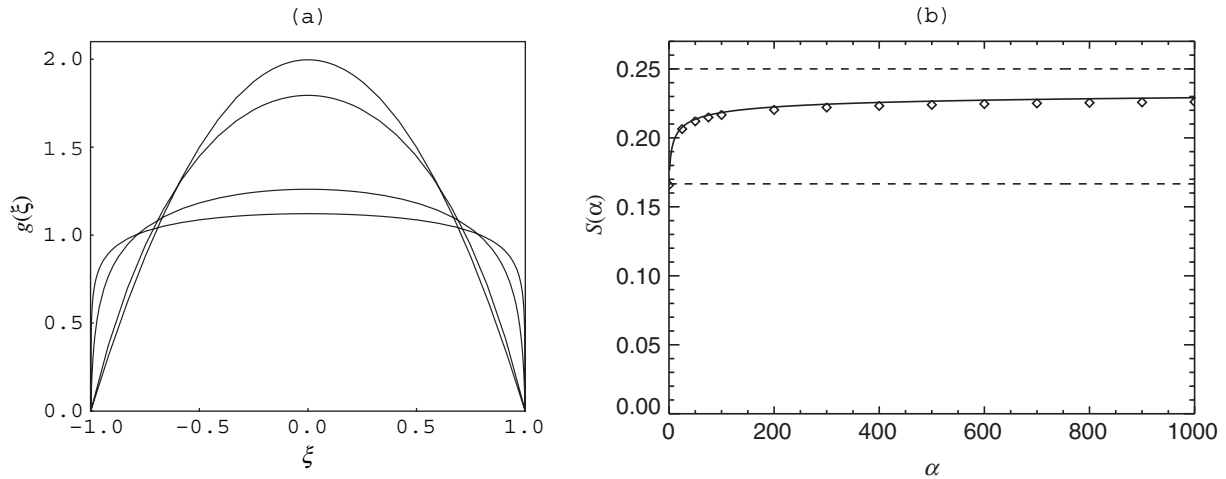
Figure 2. Sensitivity of the longitudinal flux flowmeter: (a) model profiles given by equation (19) and (b) sensitivity $S(\alpha)$ according to equation (20). The model profiles are plotted for $\alpha = 10^{-2}, 10^{0}, 10^{2}, 10^{4}$ (from top to bottom). The diamonds (right) represent the sensitivity computed numerically (see section 3.2 for details).

3.2. Numerical simulation for turbulent flows

The analytical computations of the previous section show that for a given flow rate $\pi R^2 v_0$, the Lorentz force is rather insensitive to the actual shape of the averaged velocity profile (at least for typical values of the Reynolds number encountered in metallurgical applications). In this section we investigate the following two questions: how strong is the influence of turbulent fluctuations on the time signal of the Lorentz force? How good is the kinematic approximation in comparison with a full theory that takes the back-reaction of the Lorentz force on the flow into account? To answer these questions, a numerical simulation of the pipe flow is performed using the code CDP developed at the Center for Turbulence Research (NASA Ames/Stanford Univ.) [20, 21]. In this code, the incompressible Navier–Stokes equations are spatially discretized using the finite volume method and the time advancement of the flow is performed using Crank–Nicholson scheme. The Lorentz force acting on the flow is incorporated in the algorithm as an explicit contribution to the momentum equation.

We perform two series of direct numerical simulations of the Navier–Stokes equations for the turbulent flow in a circular pipe. In the first series we address the kinematic problem, whereas the second series is devoted to the dynamic problem. In both cases we assume that the magnetic Reynolds number is small. Indeed, for the flow of a liquid metal with a magnetic diffusivity $(\mu_0\sigma)^{-1} = 1\,\mathrm{m}^2\mathrm{s}^{-1}$ and a mean velocity $v = 1\,\mathrm{ms}^{-1}$ in a pipe with radius $R = 0.01\,\mathrm{m}$ the magnetic Reynolds number is as small as $Rm = 10^{-2}$. (The magnetic diffusion time $\mu_0\sigma R^2$ is only 0.1 millisecond in this case.) To evaluate the Lorentz force acting on the magnet system we invoke the reciprocity principle (4) which reduces the task to an integration of the Lorentz force density $\mathbf{j} \times \mathbf{B}$ over the volume of the fluid. No computation of the secondary magnetic field and no integration over the coil are then necessary. By virtue of our assumption $Rm \ll 1$ we can use the (unperturbed) primary magnetic field $\mathbf{B}(\mathbf{r})$ given by (13). The secondary electric current density $\mathbf{j}(\mathbf{r})$ is computed by solving the Poisson equation (9) using the turbulent velocity field from the
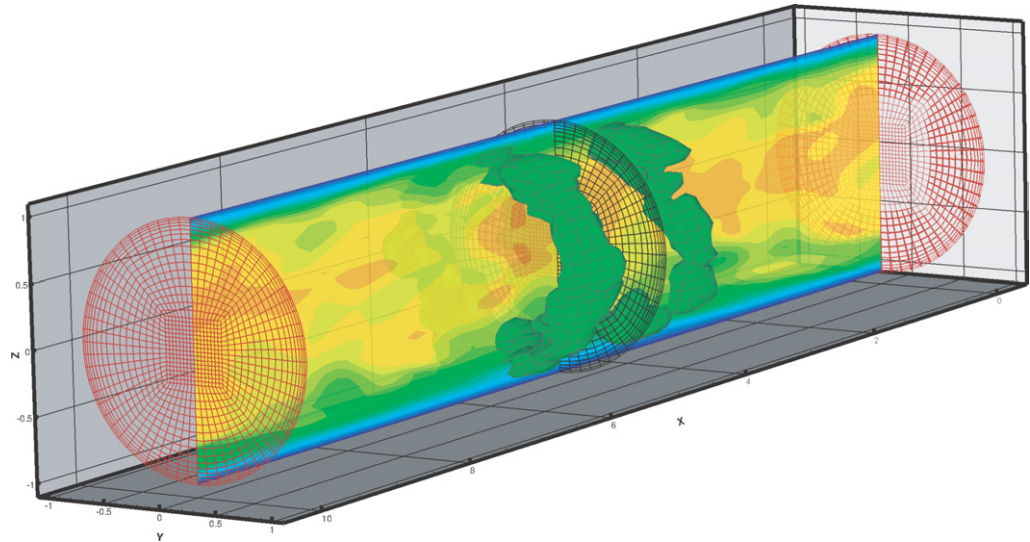
Figure 3. Lorentz force distribution in a kinematic simulation: iso-contours of the Lorentz force density in the region of space where it is the strongest. The contours of the streamwise velocity in an axial cross-section are shown.

solution of the Navier–Stokes equations, and inserting the resulting electric field $\mathbf{E} = -\nabla\Phi$ into Ohm's law (8). In the kinematic simulations we solve the Navier–Stokes equations without any Lorentz force, whereas in the dynamic simulations we solve the Navier–Stokes equations with the Lorentz force density $\mathbf{j} \times \mathbf{B}$ added to the right-hand side. The parameters of the simulations are given next.

The computational domain used in this section has an aspect ratio of 10.0 (length/radius) and is discretized using 101 648 elements. The flow is driven by a constant pressure gradient at an approximate Reynolds number $Re = 2v_0R/\nu = 3600$ where R is the radius of the pipe and ν the viscosity of the fluid. The primary magnetic field $\mathbf{B}(\mathbf{r})$ is given by (13) with $L = 2R$, i.e. the radius of the magnetic coil is twice the radius of the pipe. To avoid extra complexity, a periodic boundary condition is imposed in the streamwise direction; at the cylinder's wall, a no-slip boundary condition is imposed. For the transient cases discussed below, the flow is initialized with a turbulent-like profile on to which perturbations are superposed; the results shown are obtained after this initial state has converged to a fully developed turbulent regime.

In order to verify the magnetohydrodynamics (MHD) module developed for the CDP code, a first set of computations is performed in which the velocity profile is *prescribed* by equation (19). The sensitivity function obtained in this fashion is displayed in figure 2(a) along with the analytical result (20). It is observed that the numerically computed sensitivity lies within 1.5% of the analytical predictions for the whole range of parameters α explored. (A similar validation of the MHD module for the transverse flux flowmeter to be discussed in the next section is also performed and shows that in that case the sensitivity lies within 0.5% of the values computed analytically.)

We start our investigation with a kinematic simulation in which the Lorentz force is computed from the full three-dimensional time-dependent velocity field but does not appear on the right-hand side of the Navier–Stokes equation. Figure 3 shows an iso-contour plot of the Lorentz force density for a given instantaneous velocity field. The figure shows that the areas of strong
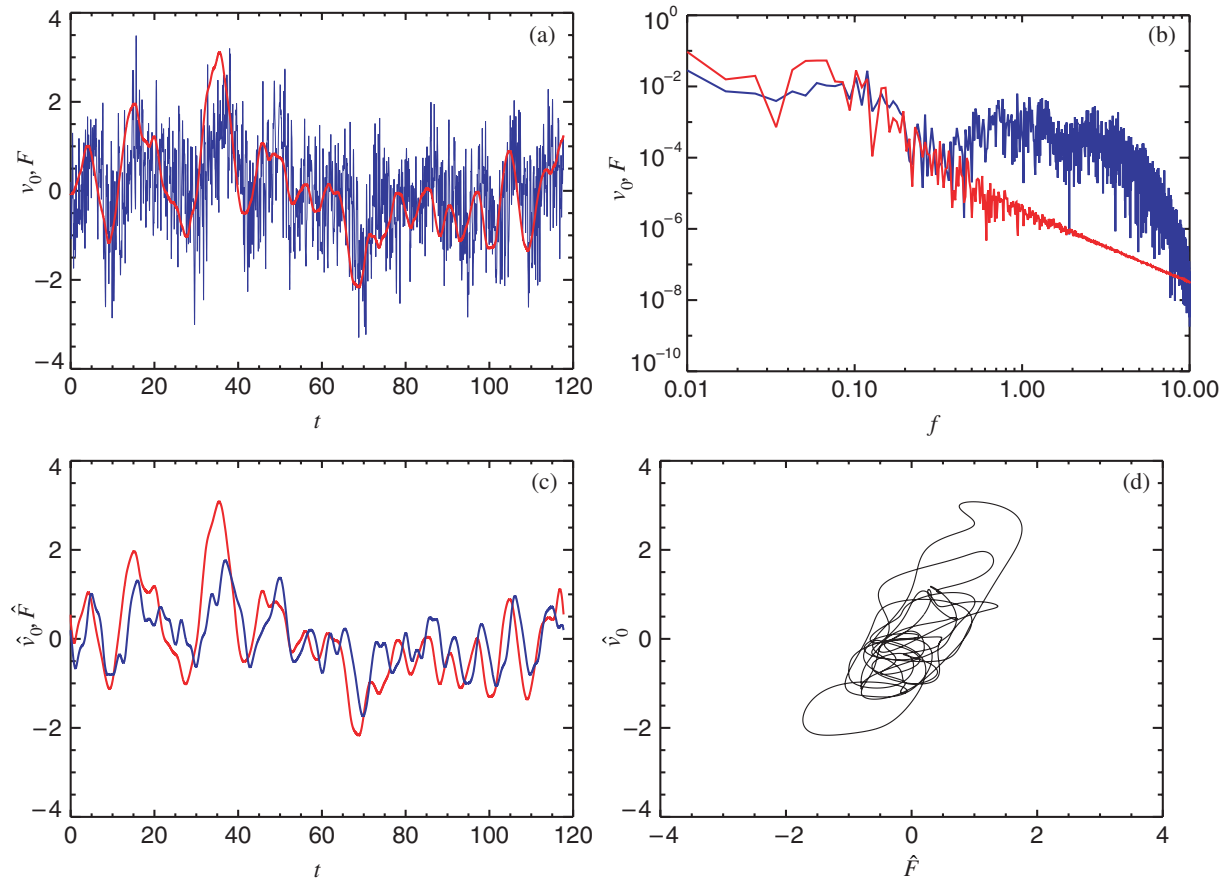
Figure 4. Results of the kinematic simulation: time history (a) and spectra (b) of the cross-section averaged velocity $v_0(t)$ (red) and of the total Lorentz force $F(t)$ (blue). (c) Low-pass filtered velocity $\hat{v}_0(t)$ (red) and force $\hat{F}(t)$ (blue); (d) scatterplot of $\hat{F}(t)$ versus $\hat{v}_0(t)$.

Lorentz force form two toroidal structures in the vicinity of the coil. This is due to the fact that the dominant contribution to the Lorentz force density comes from the interaction of the longitudinal component of the velocity with the radial component of the magnetic field, the latter having maxima upstream and downstream of the magnetic coil.

As mentioned above, the flow is sustained using a constant pressure gradient and the instantaneous flow rate thus slowly varies with time. This is illustrated in figure 4(a) in which the time series of the average velocity and the Lorentz force are plotted. Note that the signals have been normalized by removing their mean and dividing them by their standard deviations. The figure clearly shows that the Lorentz force behaviour is characterized by strong high-frequency oscillations. The physical origin of these rapid oscillations is easily understood when one recalls that in the case of the longitudinal flux flowmeter, the magnetic field is quite strongly localized in the vicinity of the plane of the coil and samples more intensively the near wall structures (see also equation (14) and the r^3 dependence of the Lorentz force). Therefore, the Lorentz force varies rapidly as the mean flow sweeps turbulent eddies across the region of intense magnetic field. On the contrary, the flow rate is obtained by integration over the flow domain, so the effect of separate local velocity fluctuations is averaged out.

To gain further insight into the nature of the high-frequency oscillations of the Lorentz force, the spectra of the time series shown in figure 4(a) are displayed in figure 4(b). Note that the frequency is normalized by $\langle v_0(t) \rangle / L$ which is the inverse of the average crossing time through the pipe. Because of the limited sampling available, the spectra inevitably appear very noisy. Nevertheless, several valuable informations can be deduced from them. At low frequencies, the figure indicates that both spectra are very similar. At higher frequencies, the amplitudes of the modes corresponding to the Lorentz force are significantly larger than those of the average velocity; this observation is completely in line with the above discussion. Worth noting are also the two peaks present in the Lorentz force spectrum at $f \approx 1$ and $f \approx 4$. The first peak is not physical and can be attributed to the fact that the simulation uses periodic boundary conditions in the streamwise direction. For this reason, the Lorentz force signal is necessarily more correlated with itself at a frequency corresponding to the inverse of the average crossing time ($f = 1$). The second peak has a physical origin and is related to the structure of the velocimeter. Indeed, a turbulent structure influences the Lorentz force signal twice as it crosses successively the two toroidal 'active' regions of the velocimeter (see figure 3). Since the separation between these two regions of space is roughly $L/4$, the natural frequency for this correlation in the Lorentz force signal is $f \approx 4$.

Because of the similarity of the spectra at low wavenumbers, it is interesting to filter the normalized signals by retaining their Fourier modes up to a frequency at which the respective spectra appear to strongly deviate. This cut-off frequency is of course not well-defined but based on figure 4(b), the value $f = 0.4$ seems a reasonable choice. The filtered normalized signals, respectively $\hat{v}_0(t)$ and $\hat{F}(t)$, are plotted in figure 4(c) and indeed appear very similar. As a further illustration, figure 4(d) shows the scatter plot of the values of $\hat{F}(t)$ and $\hat{v}_0(t)$ sampled with a certain time interval. The correlation between the two signals is beyond doubt, which is also shown by the value of the correlation coefficient $C = 0.69$. This is a positive result that demonstrates potential capability of the Lorentz force flowmeter to register fluctuations of the flow rate.

One can also notice in figure 4(c) that there is a certain time shift between the flow rate and the measured force. The oscillations in the flow rate are preceded by corresponding low-frequency oscillations of the force. An explanation of this phenomenon would require much closer scrutiny of the velocity and force fields and is beyond the scope of the present investigation. One can speculate, however, that the shift is related to evolution of near-wall coherent structures which can affect the flow rate and later be registered by the magnet system. It can be noted that in low-Re turbulent flows, such as the one analyzed in this section, the coherent structures are typically quite strong.

After having characterized the kinematic properties of the Lorentz force, we would now like to know how strongly the flow modification caused by the presence of the external magnetic field affects the measured Lorentz force. In order to answer this question we perform a second simulation in which the Lorentz force acts on the velocity field and this case therefore constitutes a complete (dynamic) MHD simulation of the flux flowmeter. For this run, the parameters are chosen in such a way that the interaction parameter, which measures the relative strength of the Lorentz force to inertial effects, is approximately equal to $N = (2\sigma B_0^2 R)/(\rho v_0) = 0.2$ where ρ is the density of the fluid. This value of N is typical of metallurgical applications. Figure 5 shows the results of the computation. As expected, the mean velocity v_0 is slightly smaller in the MHD case since extra dissipation is introduced by the Lorentz force while the forcing is identical to the one used in the kinematic case. The mean Lorentz force is also slightly smaller than in the kinematic case. Although we have not systematically studied the dynamic case,
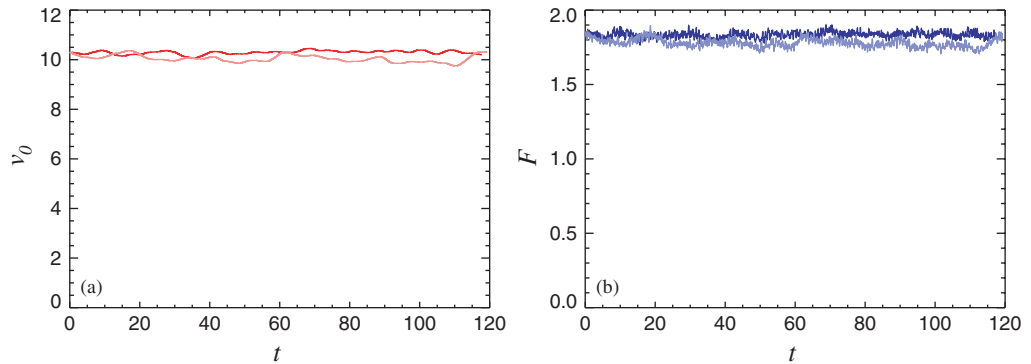
Figure 5. Dynamic versus kinematic simulations: time histories of: (a) average velocity v_0 and (b) integrated Lorentz force F for the unsteady turbulent flow in a pipe interacting with a longitudinal flux flowmeter. Both plots contain the kinematic (dark lines) and dynamic (light lines) cases.

it can be inferred from the simulation that the kinematic theory overestimates the Lorentz force but (for parameter values relevant to metallurgical applications) does not introduce a significant error into the predictions.

4. Transverse flux flowmeter

It is often desirable to use magnetic systems which are located on one side of the pipe only and whose magnetic field is predominantly transverse to the direction of the mean flow. We shall term such systems transverse flux flowmeters. Unlike longitudinal flux flowmeters which encircle the flow entirely, they do not have to be disassembled and reassembled when they are to be used in different locations.

To develop a general understanding of the main characteristics of transverse flux flowmeters we consider a steady unidirectional pipe flow with the same general velocity profile (equation (7)) as in the previous section. We wish to investigate the effect of two-dimensional magnetic fields of the form

$$\mathbf{B} = B_y(y, z)\mathbf{e}_y + B_z(y, z)\mathbf{e}_z. \tag{21}$$

Here $x = r \cos \varphi$ and $y = r \sin \varphi$ are Cartesian coordinates in the plane perpendicular to the pipe axis which we shall use in addition to the cylindrical coordinates introduced in the previous section. The components of the magnetic field must satisfy the condition $\partial B_y/\partial y + \partial B_z/\partial z = 0$ but can otherwise be arbitrary. We are interested in the streamwise component of the Lorentz force which is not affected by B_z. We therefore only need to prescribe the transverse component B_y.

To keep the analysis simple, we assume that the variation of this quantity over the cross-section of the pipe $-R \leqslant y \leqslant +R$ is weak in which case the dependence of B_y on y can be neglected. This corresponds to the case when the distance between the source of the magnetic field and the pipe is much larger than the diameter of the pipe. Hence we can write $B_y(y, z) \approx B(z)$

inside the pipe. Having in mind that any distribution $B(z)$ can be expanded into a Fourier series it is natural to start with the simplest case

$$B(z) = B_0 \cos kz, \tag{22}$$

which is also of interest as the simplest model describing the spatially periodic distribution of the magnetic field in a rotary flowmeter.

For the present case the electric potential does no longer vanish and has to be obtained by solving equation (9)

$$\nabla^2 \Phi = -B_0 \cos kz \cos \varphi \frac{\mathrm{d}v}{\mathrm{d}r} \tag{23}$$

with the boundary conditions

$$\Phi = 0 \quad (\text{for } r = 0), \qquad \frac{\partial \Phi}{\partial r} = 0 \quad (\text{for } r = R). \tag{24}$$

The first boundary condition ensures that the electric potential is unique and the electric current is nonsingular at the origin, whereas the second boundary condition expresses that the normal component of the electric current vanishes at the wall which we assume to be electrically insulating. It has to be stressed that the second condition is valid only if the flow satisfies the no-slip condition at the wall. In other cases, for example, in the case of solid-body translation considered below, the condition has to be modified to

$$\frac{\partial \Phi}{\partial r} = (\mathbf{u} \times \mathbf{B})_r \qquad (\text{for } r = R). \tag{25}$$

The solution of (23) can be represented as

$$\Phi(r, \varphi, z) = -v_0 B_0 R \cos kz \cos \varphi \cdot f\left(\frac{r}{R}\right) \tag{26}$$

where $f(\xi)$ is a solution of the equation

$$\xi^2 f'' + \xi f' - (\kappa^2 \xi^2 + 1) f = \xi^2 g'(\xi) \tag{27}$$

with the boundary conditions $f(0) = 0$ and $f'(1) = 0$. In (27), $g(\xi)$ is the shape function of the velocity profile defined in the previous section and $\kappa = kR$ is the nondimensional wavenumber of the magnetic field. Once this equation has been solved, the Lorentz force density

$$\mathbf{F} = \sigma(-\nabla\Phi + \mathbf{v} \times B) \times \mathbf{B} \tag{28}$$

can be evaluated. As in the previous section, we are only interested in the z-component of the Lorentz force. Inserting (26) into (28) and integrating over the volume $\pi R^2 L$ of one period of the magnetic field (where $L_z = 2\pi/k$) we obtain the total force as

$$F = -\frac{\pi}{2}\sigma v_0 B_0^2 R^2 L_z S(\kappa). \tag{29}$$

Here the sensitivity is given by

$$S(\kappa) = 1 - f(1). \tag{30}$$

This relation shows that we only need to know the nondimensional potential $f(1)$ at the wall of the pipe in order to compute S. In contrast to the case considered in the previous section, the sensitivity does not only depend on the shape of the velocity profile but also on the wavenumber κ of the magnetic field.

As in the previous section, we analyse the dependency of the force field (29) on the velocity profile. In the case of solid-body translation, the right-hand side of (27) is zero and the equation reduces to the modified Bessel equation. Since the no-slip condition is violated by such a flow, the boundary condition at $\xi = 1$ changes to $f'(1) = 1$ (see (25)). The solution and the sensitivity function (30) are easy to find in terms of the modified Bessel functions

$$f(\xi) = \frac{I_1(\kappa\xi)}{\kappa I'_1(\kappa)}, \qquad S(\kappa) = \frac{\kappa I_0(\kappa) - 2I_1(\kappa)}{\kappa I'_1(\kappa)} \tag{31}$$

where $\kappa I'_1(\kappa) = \kappa\,\mathrm{d}I_1(\kappa)/\mathrm{d}\kappa = \kappa I_0(\kappa) - I_1(\kappa)$. In the case of a laminar pipe Poiseuille flow with $g(\xi) = 2(1 - \xi^2)$ the equation (27) with homogeneous boundary conditions can be solved analytically as

$$f(\xi) = -\frac{4I_1(\kappa\xi)}{\kappa^3 I'_1(\kappa)} + \frac{4\xi}{\kappa^2}, \qquad S(\kappa) = 1 + \frac{4I_1(\kappa)}{\kappa^3 I'_1(\kappa)} - \frac{4}{\kappa^2}. \tag{32}$$

No analytical solution could be found for the case of the more general one-parameter velocity profile (19) so we had to resort to numerical solution. The boundary-value problem was solved using a shooting procedure based on the adaptive step-size Runge–Kutta algorithm of predetermined solution accuracy. Asymptotic expansion was used to treat the singular point at $\xi = 0$.

The results are presented in figure 6. One can see that, as in the case of longitudinal flowmeter, the measured force is weakly affected by the details of the flow field. Vastly different velocity profiles illustrated in figure 2 generate only slightly different sensitivity functions.

In addition to the total Lorentz force one is often interested in the mean Lorentz force density $f = F/(\pi R^2 L_z)$ which is equal to

$$f = \tfrac{1}{2}\sigma v_0 B_0^2 S(\kappa). \tag{33}$$

Figure 6 shows that the sensitivity of the flowmeter is a monotonically increasing function of the wavenumber. For small wavenumbers the magnetic field depends only weakly on z, the eddy currents are predominantly in the x–y-plane and their contribution to the force is small. As the wavenumber grows the eddy currents become more and more three-dimensional and the Lorentz force increases. However, one should be wary of drawing conclusions from the monotonic nature of $S(\kappa)$ without taking into account that in practice the magnetic field amplitude B_0 is not a constant. To be specific, assume that the magnetic field (22) were produced by a thin sheet of electric current with thickness δ located at a distance D below the pipe whose current density
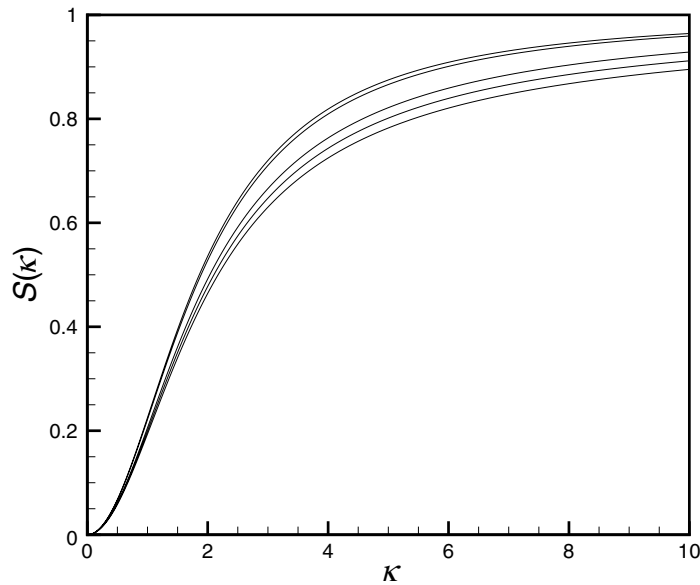
Figure 6. Sensitivity of the transverse flux flowmeter: sensitivity function $S(\kappa)$ plotted as a function of κ for the parabolic Poiseuille profile, generalized profiles (19) with $\alpha = 10^0, 10^2, 10^4$, and solid-body translation (from top to bottom). The sensitivity function obtained at $\alpha = 10^{-2}$ is indistinguishable from the function for the parabolic profile.

is given by $\mathbf{J} = J_0 \sin(kz)\mathbf{e}_x$ (for $-D - \delta/2 \leqslant y \leqslant -D + \delta/2$) and $\mathbf{J} = 0$ elsewhere. In the limit $k\delta \to 0$ (very thin sheet) the transverse magnetic field produced by the sheet is

$$B_y(y, z) = \mu_0 J_0 \delta \, e^{-k|y-D|} \cos kz. \tag{34}$$

If we further assume that the power consumption for producing the electric current, expressed in terms of dissipated Joule heat per unit length $q = (J_0^2/\sigma) \cdot 2\pi\delta/k$ is prescribed, we can write the current density as $J_0 = (\sigma k q/2\pi\delta)^{1/2}$ and the amplitude of the magnetic field becomes

$$B_0^2 = \frac{\mu_0^2 \sigma q \delta}{2\pi} k \, e^{-2kD}. \tag{35}$$

This relation shows that the magnetic field amplitude decreases strongly for large wavenumbers, so for a given electric power q (per unit length of the pipe) the Lorentz force has a maximum at a certain finite value of κ. This example demonstrates how important it is to take the source of the magnetic field properly into account.

5. Interaction of a magnetic dipole with a uniformly moving fluid

It has become obvious in the previous section that it is not only important to compute the force acting on the fluid but also to take into account the way in which the magnetic field is produced. Indeed, the sensitivity of a static Lorentz force flowmeter using permanent magnets is determined by the ratio F/M of the Lorentz force to the mass of the magnet system rather
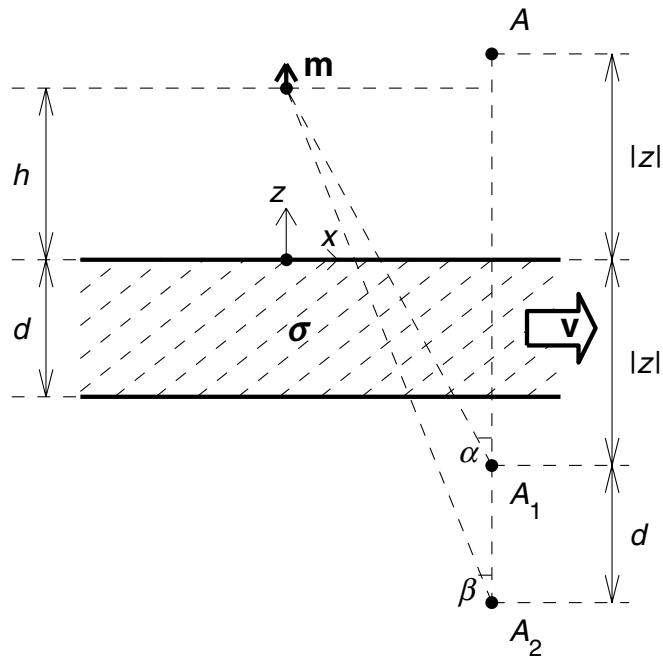
Figure 7. Sketch of the considered problem: a uniformly moving fluid with electrical conductivity σ interacts with a magnetic dipole whose orientation is perpendicular to the surface. Points A, A_1, A_2 are shown to explain the calculation of the secondary magnetic field. A is the point at which the field is to be determined, A_1 is its mirror image with respect to the plane $z = 0$, A_2 is a shift of A_1 by d in the negative z-direction.

than by the sensitivity alone. We therefore need not only a tool to compute the Lorentz force but also to relate the force to the weight of the magnet system. The present section uses an exactly solvable simplified model to outline how to accomplish this task.

5.1. Primary magnetic field

Consider a single dipole with magnetic dipole moment $\mathbf{m} = m\mathbf{e}_z$ which is located at a distance h above a fluid layer with thickness d. As shown in figure 7, the layer moves with uniform horizontal velocity $\mathbf{v} = v\mathbf{e}_x$ and extends from $z = -d$ to $z = 0$. Since we have seen in the previous sections that the Lorentz force for solid-body translation differs only weakly from that for realistic velocity profiles, we believe that this highly simplified 'flow field' captures the general properties of the problem. We will use both Cartesian coordinates x, y, z and cylindrical coordinates $x = r \cos \varphi$, $y = r \sin \varphi$ to formulate and analyse our problem. Notice that the definition of the coordinates differs from the previous two sections. Our goal is to compute the primary magnetic field $\mathbf{B}(r)$, the electric potential $\phi(\mathbf{r})$, the eddy currents $\mathbf{J}(r)$ and finally the secondary magnetic field $\mathbf{b}(r)$. In contrast to the previous two sections the force will be computed by evaluating the interaction of the secondary magnetic field with the magnetic dipole. The dipole generates a primary magnetic field whose distribution is well known from classical electrodynamics, see e.g. [18], and is

given by

$$\mathbf{B}(\mathbf{r}') = \frac{\mu_0}{4\pi} \left\{ 3(\mathbf{m} \cdot \mathbf{r}') \frac{\mathbf{r}'}{r'^5} - \frac{\mathbf{m}}{r'^3} \right\}. \tag{36}$$

Here $\mathbf{r}' = \mathbf{r} - h\mathbf{e}_z$ and $r' = |\mathbf{r}'|$. In order to compute the eddy currents, we need to know the primary field within the moving fluid. The components of this field are

$$B_x = \frac{3\mu_0 m}{4\pi} \frac{(z-h)\, r \cos\varphi}{\left[r^2 + (z-h)^2\right]^{5/2}}, \tag{37}$$

$$B_y = \frac{3\mu_0 m}{4\pi} \frac{(z-h)\, r \sin\varphi}{\left[r^2 + (z-h)^2\right]^{5/2}}, \tag{38}$$

$$B_z = \frac{\mu_0 m}{4\pi} \frac{2(z-h)^2 - r^2}{\left[r^2 + (z-h)^2\right]^{5/2}}. \tag{39}$$

5.2. Secondary electric currents

Next we need to determine the distribution of the electric potential in order to obtain the eddy currents. To this end we take the divergence of Ohm's law (8) having in mind that $\mathbf{j}$ is divergence-free and that $\nabla \cdot (\mathbf{v} \times \mathbf{B}) = \mathbf{B} \cdot (\nabla \times \mathbf{v}) - \mathbf{v} \cdot (\nabla \times \mathbf{B}) = 0$ because both the primary magnetic field and the velocity are irrotational within the layer. Thus the potential in the layer is governed by

$$\nabla^2 \Phi = 0 \tag{40}$$

for $-d < z < 0$ supplemented by the boundary conditions

$$\frac{\partial \Phi}{\partial z} = -\frac{3\mu_0 m v}{4\pi} \frac{hr \sin\varphi}{[r^2 + h^2]^{5/2}} \quad \text{at } z = 0, \tag{41}$$

$$\frac{\partial \Phi}{\partial z} = -\frac{3\mu_0 m v}{4\pi} \frac{(d+h)r \sin\varphi}{[r^2 + (d+h)^2]^{5/2}} \quad \text{at } z = -d. \tag{42}$$

These conditions express that the vertical component of the electric current density must vanish at the surfaces of the layer and are obtained by using Ohm's law (8) to write $j_z = 0$ as $\partial \phi / \partial z = v B_y(x, y, 0)$ and by using (37) to express B_y.

It can be readily verified that the solution of this problem is

$$\Phi(r, \varphi, z) = -\frac{\mu_0 m v}{4\pi} \frac{r \sin\varphi}{\left[r^2 + (z-h)^2\right]^{3/2}}. \tag{43}$$

Based on this, the secondary electric currents are immediately obtained employing (8) as

$$j_x = -\frac{3\mu_0 m \sigma v}{8\pi} \frac{r^2 \sin 2\varphi}{\left[r^2 + (z-h)^2\right]^{5/2}}, \tag{44}$$
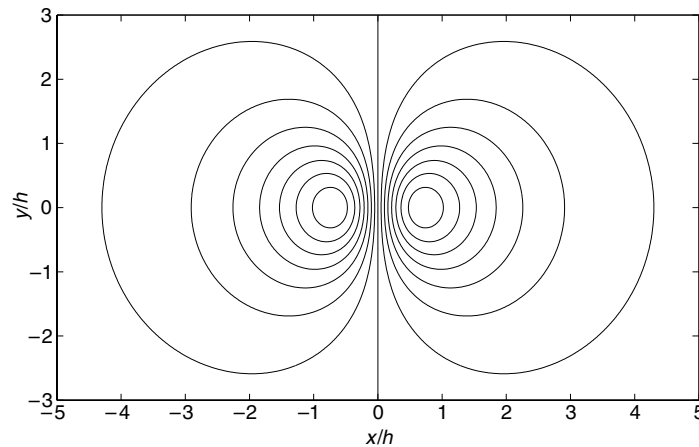
Figure 8. Distribution of eddy currents for the case when a magnetic dipole interacts with a uniformly moving fluid. The currents are shown for the upper surface ($z = 0$). The fluid moves from left to right and the eddy currents at $x = y = 0$ are in the positive y-direction.

$$j_y = -\frac{\mu_0 m \sigma v}{8\pi} \frac{2(z-h)^2 - r^2(1 + 3\cos 2\varphi)}{\left[r^2 + (z-h)^2\right]^{5/2}}, \tag{45}$$

$$j_z = 0. \tag{46}$$

These eddy currents are purely horizontal. Due to their two-dimensionality they can be expressed as $\mathbf{j} = \nabla \times (\psi \mathbf{e}_z)$ where

$$\psi(x, y, z) = \frac{\mu_0 m \sigma v}{4\pi} \frac{r \cos \varphi}{[r^2 + (z-h)^2]^{3/2}}. \tag{47}$$

The isolines of $\psi(x, y, 0)$ are plotted in figure 8. The figure shows that the secondary electric currents are strongest below the location of the dipole and form two large counterrotating eddies.

5.3. Secondary magnetic field

When $\mathbf{j}$ is time-independent, the secondary magnetic field $\mathbf{b}$ is uniquely determined by Ampere's law

$$\mathbf{j} = \frac{1}{\mu_0} \nabla \times \mathbf{b} \tag{48}$$

combined with the equation $\nabla \cdot \mathbf{b} = 0$ and the boundary condition $|\mathbf{b}| \to 0$ at infinity. The fact that the eddy currents are purely horizontal simplifies the computation of the secondary magnetic field and of the force considerably because $\mathbf{b}$ can be represented as $\mathbf{b} = \nabla \times \nabla \times (\chi \mathbf{e}_z)$ with

$$\chi(\mathbf{r}) = \frac{\mu_0}{4\pi} \int \frac{\psi(\mathbf{r}')}{|\mathbf{r} - \mathbf{r}'|} \, \mathrm{d}^3 \mathbf{r}'. \tag{49}$$
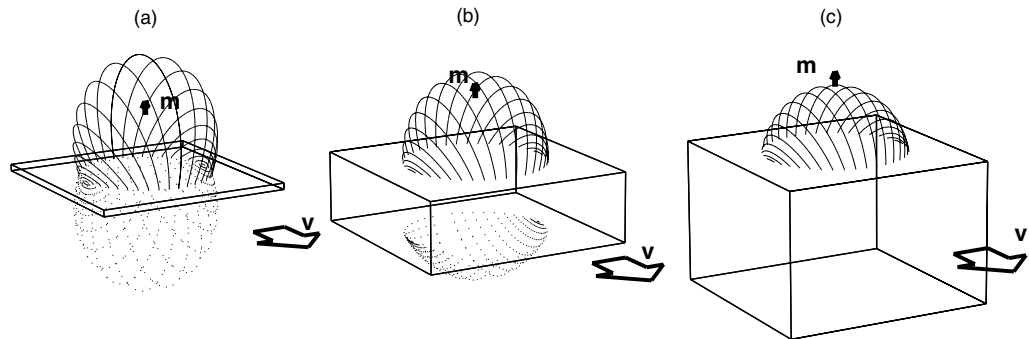
Figure 9. Structure of the secondary magnetic field induced by the interaction of a moving layer with a magnetic dipole. For clarity only a small subset of the magnetic field lines is plotted for which the field lines originate from the circle $r = h$ at $z = 0$. (a) Thin layer, (b) general case and (c) semi-infinite layer. The secondary field at the location of the dipole is in the same direction as the flow.

As detailed in the appendix, the necessary integrations can be performed analytically and lead to the following result:

$$\chi(r, \varphi, z) = \frac{\mu_0 m \sigma v}{4} \left\{ \left[\frac{\zeta(r, z, h) - 1}{\zeta(r, z, h) + 1} \right]^{1/2} - \left[\frac{\zeta(r, z, h + d) - 1}{\zeta(r, z, h + d) + 1} \right]^{1/2} \right\} \cos \varphi \quad (50)$$

where $\zeta(r, z, \ell) = [1 + r^2/(\ell + |z|)^2]^{1/2}$. Figure 7 shows that the functions $\zeta(r, z, h)$ and $\zeta(r, z, h + d)$ have clear geometrical meaning. Let A be an arbitrary point at which the field is to be computed, A_1 its mirror-image with respect to the plane $z = 0$, and A_2 its shift by $-d$ along the z-direction. Then, $\tan(\alpha) = r/(|z| + h)$ and $\tan(\beta) = r/(|z| + h + d)$, where the angles α and β are shown in figure 7. Hence, $1/\zeta(r, z, h) = \cos(\alpha)$ and $1/\zeta(r, z, h + d) = \cos(\beta)$, and after some algebra we arrive at the compact form

$$\chi(r, \varphi, z) = \frac{\mu_0 m \sigma v}{4} \{\tan(\alpha/2) - \tan(\beta/2)\} \cos \varphi. \quad (51)$$

The structure of χ shows that the magnetic field of a layer with finite thickness d is the same as that of two semi-infinite layers moving in opposite directions where one layer has its surface at $z = 0$ and moves in positive direction while the surface of the other layer is located at $z = -(h + d/2)$ and moves in the negative x-direction.

From expression (48) the secondary magnetic field is readily obtained by differentiation: $b_x = \partial^2 \chi/\partial x \partial z$, $b_y = \partial^2 \chi/\partial y \partial z$, $b_z = -\partial^2 \chi/\partial x^2 - \partial^2 \chi/\partial y^2$. Since the resulting expressions are lengthy we will not write them out explicitly. The structure of the secondary magnetic field is shown in figure 9.

For the particular cases of a thin layer ($d \ll h$) and a thick layer ($d \gg h$) the magnetic field can be written explicitly. Details of the derivations are given in the appendix. For the thin layer

we obtain

$$b_x(r, \varphi, z) = \frac{\mu_0^2 m \sigma v}{8\pi} \frac{\sin^3(\alpha)}{r^3} \left[3 \sin^2(\alpha) \cos^2(\varphi) - 1 \right] \text{sign}(z),$$

$$b_y(r, \varphi, z) = \frac{\mu_0^2 m \sigma v d}{16\pi} \frac{3 \sin^5(\alpha)}{r^3} \sin(2\varphi) \, \text{sign}(z), \tag{52}$$

$$b_z(r, \varphi, z) = \frac{\mu_0^2 m \sigma v d}{8\pi} \frac{3 \sin^5(\alpha)}{r^3} \cos(\varphi),$$

whereas for the thick layer we have

$$b_x(r, \varphi, z) = \frac{\mu_0^2 m \sigma v}{16\pi} \frac{\sin^2(\alpha/2)}{r^2} \left[4 + 3 \cos(\alpha) + \cos^2(\alpha) \right] \cos(2\varphi) \, \text{sign}(z),$$

$$b_y(r, \varphi, z) = \frac{\mu_0^2 m \sigma v}{8\pi} \frac{\sin^2(\alpha/2)}{r^2} (2 + \cos \alpha) \sin(2\varphi) \, \text{sign}(z), \tag{53}$$

$$b_z(r, \varphi, z) = \frac{\mu_0^2 m \sigma v d}{16\pi} \frac{\sin^3(\alpha)}{r^2} \cos(\varphi).$$

Both distributions are shown in figure 9 as well.

5.4. Force and torque

In sections 2 and 3 we have computed the force on the magnet system by evaluating the force on the fluid and by invoking the reciprocity principle (4). Here we illustrate the alternative route which consists of computing the force on the magnetic dipole directly by making use of the secondary magnetic field. The advantage of this approach is that it provides us not only with the force but furnishes the torque on the magnet system as well.

According to classical electrodynamics (see e.g. [18]) our magnetic dipole experiences a force

$$\mathbf{F} = (\mathbf{m} \cdot \nabla)\mathbf{b} \tag{54}$$

and a torque

$$\mathbf{T} = \mathbf{m} \times \mathbf{b} \tag{55}$$

due to the secondary magnetic field. Along the axis $r = 0$ where the dipole is located, b_x is the only nonvanishing component, as can be seen from figure 9. Consequently, only the components $F_x = m \partial b_x(0, 0, z)/\partial z|_{z=h}$ and $T_y = m b_x(0, 0, h)$ are nonzero. In order to compute these quantities we need to know $\mathbf{b}$ along the line $r = 0$. These computations can be performed analytically and provide the result

$$\mathbf{F} = + \frac{1}{128\pi} \cdot \frac{\mu_0^2 m^2 \sigma v}{h^3} S_F(\delta)\mathbf{e}_x, \tag{56}$$

$$\mathbf{T} = - \frac{1}{128\pi} \cdot \frac{\mu_0^2 m^2 \sigma v}{h^2} S_T(\delta)\mathbf{e}_y, \tag{57}$$

where the sensitivities $S_F(\delta)$ and $S_T(\delta)$ as functions of the nondimensional plate thickness $\delta = d/h$ are given by

$$S_F(\delta) = 1 - \frac{1}{(1+\delta)^3}, \tag{58}$$

$$S_T(\delta) = 1 - \frac{1}{(1+\delta)^2}. \tag{59}$$

For a thin layer ($\delta \to 0$) we readily obtain

$$S_F = 3\delta, \qquad S_T = 2\delta, \tag{60}$$

whereas for the semi-infinite layer ($\delta \to \infty$) we have

$$S_F = 1, \qquad S_T = 1. \tag{61}$$

These expressions display several important properties of Lorentz force flowmeters. Firstly, the torque and the force are proportional to the velocity and to the square of the magnetic dipole moment. This shows that the sensitivity of a Lorentz force flowmeter is a nonlinear function of the intensity of the primary magnetic field in contrast to conventional inductive flow measurement methods like inductive flowmeters or inductive flow tomography. The sensitivity of Lorentz flowmeters can therefore be greatly enhanced by selecting magnetic materials with high magnetization. Secondly, the torque given by equation (57) is negative. If the dipole were of finite extent and free to rotate about the y-axis, it would rotate in the same way as a flywheel forced by the flow. The positive sign of the force shows that the fluid drags the magnetic dipole along its own direction of motion. These facts support our intuitive view that the flow invisibly rotates and drags the dipole as if the dipole's magnetic field lines would feel a friction with the flow. Finally, both the torque and the force decay quickly with increasing distance, whereby the decay of the force ($F_x \sim h^{-4}$) is faster than the decay of the torque ($T_y \sim h^{-3}$).

It should be noted that the force increases more quickly with increasing thickness of the layer than the torque. This property has an interesting consequence, illustrated by dot-dashed line in figure 10 which presents the ratio of the force and the torque (in nondimensional form $S_F(\delta)/S_T(\delta)$). This quantity is a monotonically decreasing function of δ which implies that if one simultaneously measures both the force and the torque one can not only determine the velocity but also the thickness of the layer. Indeed, from the ratio

$$\frac{S_F(\delta)}{S_T(\delta)} = \frac{3 + 3\delta + \delta^2}{2 + 3\delta + \delta^2} \tag{62}$$

one can determine δ which can then be used in (57) or (56) to obtain the velocity.

Let us illustrate the predictions of the theory using a practical example. Consider a cubic permanent magnet with 1 cm side length consisting of magnetic material with magnetization density $M = 2000 \, \text{kA m}^{-1}$. The volume of the magnet is $V = 10^{-6} \, \text{m}^3$, and its magnetic moment becomes $m = MV = 2 \, \text{A m}^2$. At a distance $h = 1.5 \, \text{cm}$ from the magnet we imagine three layers of liquid metal with thicknesses $d_1 = 1 \, \text{mm}$, $d_2 = 1 \, \text{cm}$, and $d_3 = 10 \, \text{cm}$ having electrical conductivity $\sigma = 10^6 \, (\Omega \, \text{m})^{-1}$ moving with velocity $v = 1 \, \text{ms}^{-1}$. Then, gathering all parameters into (56) and remembering that $\mu_0 = 4\pi \times 10^{-7} \, \text{NA}^{-2}$ we obtain the forces
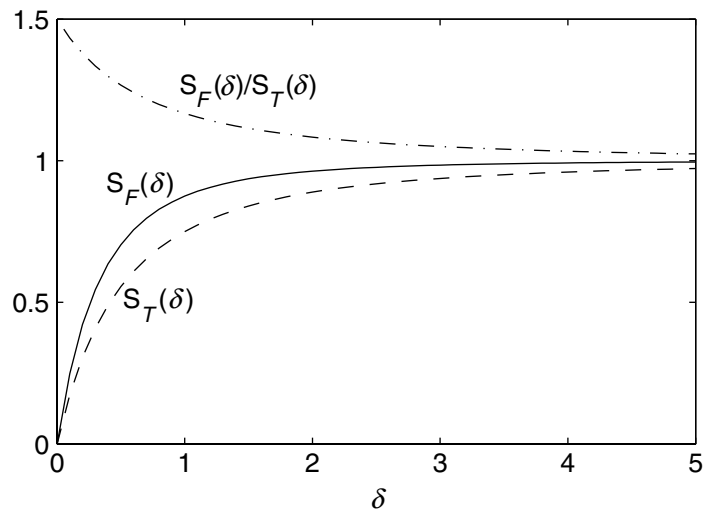
Figure 10. Force and torque on a uniformly moving fluid layer interacting with a magnetic dipole: sensitivity of force (solid line), sensitivity of torque (dashed line) and their ratio (dot-dashed line) as a function of $\delta = d/h$ as obtained from equations (58), (59) and (62), respectively.

$F_1 = 1.3935 \times 10^{-5}\,\text{N}$, $F_2 = 1.3688 \times 10^{-4}\,\text{N}$, and $F_3 = 0.012\,\text{N}$ respectively. This example shows that the force becomes very small when the fluid layer is thin. Notice, however, that it is not the absolute force which is important but rather the ratio of the Lorentz force to the gravity force acting on the magnet. These ratios are approximately 3×10^{-4}, 3×10^{-3} and 0.25, respectively.

6. General kinematic theory

Having developed a sufficient intuitive understanding of the physical principles of the Lorentz force flowmeter, we can now summarize the general mathematical formulation of the theory. The general problem can be formulated as follows: given a magnet system characterised by a spatial distribution $\mathbf{J}(\mathbf{r})$ of the primary electric currents or by a distribution $\mathbf{M}(\mathbf{r})$ of magnetization density and given a (possibly time-dependent) velocity field $\mathbf{v}(\mathbf{r})$ compute the force $\mathbf{F}$ and the torque $\mathbf{T}$ acting on the magnet system. In formulating the theory we should once again emphasize the distinction between the *kinematic problem* in which the velocity field is prescribed and the *dynamic problem* where the velocity field is modified by the presence of the primary field and has to be determined as a solution of the equations of MHD. Here we will formulate the kinematic theory. To this end we shall make the following assumptions.

Firstly, we assume that the velocity field is known. This is a less restrictive assumption than it might appear. Indeed, the kinematic theory is valid no matter whether the velocity field is prescribed (as in the previous sections) or determined by solving the equations of MHD. Secondly, we shall suppose that the primary magnetic field is much stronger than the secondary field. This is expressed by the condition that the magnetic Reynolds number $Rm = \mu_0 \sigma v L$ is small—a condition that is met in most industrial applications of electrically conducting fluids. Thirdly, the typical time scale T of the large-scale structures of the flow is assumed to be much

larger than the magnetic diffusion time $\mu_0 \sigma L^2$; this allows us to use the quasistatic approximation for the computation of the secondary magnetic field. Fourthly, we restrict our attention to the case where the sources of the magnetic field $\mathbf{J}(\mathbf{r})$ or $\mathbf{M}(\mathbf{r})$ are given. In case of a permanent-magnet system this means that the permanent magnets consist of hard magnetic material which implies that the distribution of magnetization density is unaffected by the primary or secondary magnetic field. Finally, we exclude the possibility that the magnetic system moves under the influence of the force and torque, thereby sacrificing magnetic fluid–structure interactions.

6.1. Primary magnetic field

When the magnet system is an electromagnet with an electric current distribution $\mathbf{J}(r)$ the corresponding primary magnetic field is given by Biot–Savart's law

$$\mathbf{B}(\mathbf{r}) = \frac{\mu_0}{4\pi} \int \frac{\mathbf{J}(\mathbf{r}') \times (\mathbf{r} - \mathbf{r}')}{|\mathbf{r} - \mathbf{r}'|^3} \, \mathrm{d}^3 \mathbf{r}'. \tag{63}$$

The case of a system of permanent magnets characterized by a distribution $\mathbf{M}(r)$ of magnetization density can be treated in the same way if we introduce a fictitious electric current distribution

$$\mathbf{J} = \nabla \times \mathbf{M}. \tag{64}$$

Sometimes, however, it is more convenient to use the equations of magnetostatics (see e.g. [22])

$$\nabla \times \left(\frac{\mathbf{B}}{\mu_0} - \mathbf{M} \right) = 0, \qquad \nabla \cdot \mathbf{B} = 0. \tag{65}$$

It follows from the first of these two equations that $\mu_0^{-1} \mathbf{B} - \mathbf{M}$ must be the gradient of a magnetic potential whose distribution inside and outside the magnet system is denoted by Ψ and Ψ_M, respectively. The second of the equations requires

$$\nabla^2 \Psi_M = -\nabla \cdot \mathbf{M} \qquad \text{within the magnet system} \tag{66}$$

and

$$\nabla^2 \Psi = 0 \qquad \text{outside the magnet system.} \tag{67}$$

The normal component of the magnetic field has to be continuous across the boundary of the magnetic system which leads to the boundary condition

$$\frac{\partial \Psi}{\partial n} - \frac{\partial \Psi_M}{\partial n} = M_n. \tag{68}$$

Here ∂/∂_n is the normal derivative and $M_n = \mathbf{M} \cdot \mathbf{n}$ the normal component of the magnetization at the *inner* boundary of the magnet system. Finally we require that there are no magnetic fields at infinity, i.e. $|\Psi| \to 0$ as $|\mathbf{r}| \to \infty$. Equations (66)–(68) uniquely determine the primary magnetic field $\mathbf{B} = \mu_0 \nabla \Psi$ within the fluid.

IOP Institute of Physics ⬧ DEUTSCHE PHYSIKALISCHE GESELLSCHAFT

6.2. Electric potential and eddy currents

To compute the eddy currents we take the divergence of Ohm's law (8), remember that $\nabla \times \mathbf{B} = 0$ in the fluid, and obtain

$$\nabla^2 \Phi = \mathbf{B} \cdot (\nabla \times \mathbf{v}) \tag{69}$$

for the electric potential. The boundary condition at the wall is obtained by requiring the normal component of the eddy currents to be zero. Using (8) this translates into

$$\frac{\partial \Phi}{\partial n} = \mathbf{n} \cdot (\mathbf{v} \times \mathbf{B}). \tag{70}$$

If we have the no-slip condition $\mathbf{v} = 0$ at the wall, this boundary condition simplifies to $\partial \Phi / \partial n = 0$. Once Φ is obtained, the eddy currents $\mathbf{j}$ can be computed from Ohm's law.

6.3. Secondary magnetic field

The eddy currents create the secondary magnetic field which is described by equation (48) and the condition $\nabla \cdot \mathbf{b} = 0$. The latter condition can be automatically satisfied by introducing the magnetic potential according to $\mathbf{b} = \nabla \times \mathbf{a}$. Inserting this into Ampere's law yields the equation

$$-\nabla^2 \mathbf{a} = \mu_0 \mathbf{j} \tag{71}$$

which has to be solved subject to the boundary condition $\mathbf{b} \to 0$ at infinity. This solution can be explicitly written down and leads to the following integral representation of the secondary magnetic field.

$$\mathbf{b}(\mathbf{r}) = \frac{\mu_0}{4\pi} \int \frac{\mathbf{j}(\mathbf{r}') \times (\mathbf{r} - \mathbf{r}')}{|\mathbf{r} - \mathbf{r}'|^3} \, d^3\mathbf{r}'. \tag{72}$$

Observe that the secondary magnetic field is a linear functional of both the velocity and current or magnetization.

6.4. Force and torque

Once the secondary magnetic field has been computed, the force and torque are obtained by integrating over the whole magnetic system. The results are

$$\mathbf{F} = \int_m [\mathbf{M}(\mathbf{r}) \cdot \nabla] \mathbf{b}(\mathbf{r}) d^3\mathbf{r} \tag{73}$$

and

$$\mathbf{T} = \int_m \mathbf{M}(\mathbf{r}) \times \mathbf{b}(\mathbf{r}) d^3\mathbf{r}. \tag{74}$$

Notice that both the torque and the force are quadratic functionals of the magnetization and linear functionals of the velocity.

7. Summary and conclusions

We have formulated the theory of Lorentz force velocimetry. The main results are embodied in the exact analytic relations (20) for the sensitivity of the longitudinal flux flowmeter with general velocity profile, (32) for the transverse flowmeter with Poiseuille profile and (58), (59) for a moving layer under the influence of a localized distribution of magnetic material. Moreover, the general equations summarized in section 6 provide a rational framework for the sensitivity analysis for complex velocimeter geometries for industrial use.

Acknowledgments

Appendix. Secondary magnetic field for a moving layer

The secondary magnetic field can be represented as $\mathbf{b} = \nabla \times \mathbf{a}$. The vector potential $\mathbf{a}$ ensures the solenoidal character of $\mathbf{b}$ and can be expressed through the secondary electric current via

$$\mathbf{a}(\mathbf{r}) = \frac{\mu_0}{4\pi} \int \frac{\mathbf{j}(\mathbf{r}')}{|\mathbf{r} - \mathbf{r}'|} \, \mathrm{d}^3 \mathbf{r}'. \tag{A.1}$$

The two-dimensionality of the current, i.e. ($\mathbf{j} = \nabla \times (\psi \mathbf{e}_z)$), permits us to express the vector potential as $\mathbf{a} = \nabla \times (\chi \mathbf{e_z})$ when

$$\chi(\mathbf{r}) = \int \frac{\psi(\mathbf{r}')}{|\mathbf{r} - \mathbf{r}'|} \mathrm{d}^3 \mathbf{r}'. \tag{A.2}$$

The final integration is carried out with the aid of the Fourier decomposition

$$\frac{1}{|\mathbf{r} - \mathbf{r}'|} = \sum_{m=0}^{\infty} \epsilon_m \cos\left[m(\varphi - \varphi')\right] \int_0^{\infty} \mathrm{e}^{-k|z-z'|} J_m(kr) J_m(kr') \, \mathrm{d}k. \tag{A.3}$$

Here, ϵ_m is the so-called Neumann symbol, defined as $\epsilon_m = 1$ for $m = 0$ and $\epsilon_m = 2$ for $m \neq 0$ and J_m are cylindrical Bessel functions of order m. Since ψ given by (47) has only one nonzero azimuthal Fourier component, the integration over the horizontal coordinates can be performed

analytically. It gives:

$$\chi(r, \varphi, z) = \frac{\mu_0 m \sigma v}{\pi} \frac{[\zeta(r, z, h) - 1]}{r\zeta(r, z, h)} \cos\varphi, \tag{A.4}$$

where $\zeta(r, z, h) = [1 + r^2/(h + |z|)^2]^{1/2}$. This expression gives χ for the infinitely thin layer moving at a distance h from the dipole. Since the eddy currents are entirely horizontal, in order to find χ for the layer of arbitrary thickness one can consider it as a collection of thin layers which are located at distances $h + z'$ where z' belongs to interval $-d \leqslant z' \leqslant 0$. In particular, for each slice having coordinate z' we perform the same calculation as before for the thin plate and obtain χ given by (A.4). First, we extract the coordinate z' of the slice: $|z| \to |z - z'|$ and $h \to h - |z'|$, where $|z|$ is the distance between point A and the upper surface located at $z = 0$, and h is the distance between the upper surface and the dipole **m**, see figure 7. In order to use (A.4), the function $\zeta(r, z, h)$ must be taken as $\zeta(r, z + |z'|, h + |z'|) = [1 + r^2/(h + |z| - 2|z'|)^2]^{1/2}$ and then (A.4) can be integrated over $-d \leqslant z' \leqslant 0$. The integration is performed conveniently by substituting z' by ζ':

$$d\zeta'(r, z + |z'|, h + |z'|) = 2\frac{(\zeta'^2 - 1)^{\frac{3}{2}}}{r\zeta'}dz',$$

and the resulting χ for the finite layer is:

$$\chi = \frac{\mu_0 m \sigma v}{\pi} \cos(\varphi) \int_{-d}^{0} \frac{2(\zeta'(z') - 1)}{\zeta'(z')r} dz' \tag{A.5}$$

$$= \frac{\mu_0 m \sigma v}{\pi} \cos(\varphi) \int_{\zeta(r,z,h+d)}^{\zeta(r,z,h)} \frac{d\zeta'}{(\zeta' - 1)^{1/2}(\zeta' + 1)^{3/2}} \tag{A.6}$$

which gives finally (50).

References

[1] Thess A, Votyakov E and Kolesnikov Y 2006 Lorentz force velocimetry *Phys. Rev. Lett.* **96** 164501
[2] Faraday M 1832 *Phil. Trans. R. Soc.* **15** 175
[3] Shercliff J A 1962 *The Theory of Electromagnetic Flow Measurement* (Cambridge: Cambridge University Press)
[4] Feng C C, Deeds W E and Dodd C V 1975 Analysis of eddy current flow meters *J. Appl. Phys.* **46** 2935–40
[5] Baumgartl J, Hubert A and Müller G 1993 The use of magnetohydrodynamic effects to investigate fluid flow in electrically conducting melts *Phys. Fluids* A **5** 3280–9
[6] Stefani F, Gundrum T and Gerbeth G 2004 Contactless inductive flow tomography *Phys. Rev.* E **70** 056306
[7] Shercliff J A 1960 *Patent* GB 831226
[8] Kawabe R 1982 *Japanese Patent* JP57199917 A
[9] Morishita M 1995 *Japanese Patent* JP 19930327846 19931224
[10] Cervantes M, Enström C, Kelvesjö H and Ohlsson H 2000 *US Patent* 6538433 B1
[11] Bucenieks I 2005 Modelling of rotary inductive electromagnetic flowmeter for liquid metals flow control *Proc. 8th Int. Symp. on Magnetic Suspension Technology, Dresden, Germany, 26–28 September* ed G Fuchs, L Schultz, O de Haas and H-J Schneider-Muntau, pp 204–8
[12] Thess A, Kolesnikov Y and Karcher C 2007 *Patent* WO 2007/033982 A1

[13] Sjörström U and Kelvesjö H 2005 Sensor for non-contact velocity measurements for continuous casting slab moulds—first results from industrial measurements *Proc. Continuous Casting Conf. (Nice, France)*

[14] Roberts P H 1967 *An Introduction to Magnetohydrodynamics* (New York: Elsevier)

[15] Moreau R 1990 *Magnetohydrodynamics* (Dordrecht: Kluwer)

[16] Davidson P A 2001 *An Introduction to Magnetohydrodynamics* (Cambridge: Cambridge University Press)

[17] Davidson P A 1999 Magnetohydrodynamics in materials processing *Annu. Rev. Fluid Mech.* **31** 273–300

[18] Jackson J D 1975 *Classical Electrodynamics* (New York: Wiley)

[19] Zagarola M V and Smits A J 1998 Mean-flow scaling of turbulent pipe flow *J. Fluid. Mech.* **373** 33–79

[20] Mahesh K, Constantinescu G and Moin P 2004 A numerical method for large-eddy simulation in complex geometries *J. Comput. Phys.* **197** 215–40

[21] Ham F and Iaccarino G 2004 Energy conservation in collocated discretization schemes on unstructured meshes *Annual Research Briefs 2004* (Center For Turbulence Research, NASA Ames/Stanford Univ.) pp 3–14

[22] Abele M G 1993 *Structures of Permanent Magnets* (New York: Wiley)